

Received April 16, 2022, accepted April 30, 2022, date of publication May 3, 2022, date of current version May 11, 2022.

Digital Object Identifier 10.1109/ACCESS.2022.3172292

# Model-Based Maximum Power Point Tracking Algorithm With Constant Power Generation Capability and Fast DC-Link Dynamics for Two-Stage PV Systems

**MOSTAFA AHMED**<sup>1,2</sup>, (Graduate Student Member, IEEE),  
**IBRAHIM HARBI**<sup>1,3</sup>, (Graduate Student Member, IEEE),  
**RALPH KENNEL**<sup>1</sup>, (Senior Member, IEEE), **JOSE RODRIGUEZ**<sup>4</sup>, (Life Fellow, IEEE),  
**AND MOHAMED ABDELRAHEM**<sup>1,2</sup>, (Senior Member, IEEE)

<sup>1</sup>Chair of High-Power Converter Systems, Technical University of Munich (TUM), 80333 Munich, Germany

<sup>2</sup>Electrical Engineering Department, Faculty of Engineering, Assiut University, Assiut 71516, Egypt

<sup>3</sup>Electrical Engineering Department, Faculty of Engineering, Menoufia University, Shebin El-Koum 32511, Egypt

<sup>4</sup>Faculty of Engineering, Universidad San Sebastian, Santiago 8370146, Chile

Corresponding author: Mostafa Ahmed (mostafa.ahmed@tum.de)

The work of Jose Rodriguez was supported by the Agencia Nacional de Investigación y Desarrollo (ANID) under Project FB0008, Project ACT192013, and Project 1210208.

**ABSTRACT** In this paper, a model-based maximum power point tracking (MPPT) technique is presented for a two-stage grid-connected photovoltaic (PV) system, where the loci of the maximum power points (MPPs) is specified accurately based on a new formulation. In this formulation, the effect of both irradiance and temperature is taken into consideration, whereas the irradiance is estimated to reduce the cost of the system and enhance its reliability. Furthermore, constant power generation (CPG) is integrated with the developed MPPT method to facilitate other power regulation schemes in the PV system. The proposed methodology is compared with the well-known perturb and observe (P&O) method for evaluation. Additionally, a modified version of the P&O is included in the comparison for better assessment. The effect of different partial shading conditions on the system's performance is also investigated. The DC-link PI controller is replaced with a new adaptive DC-link controller to enhance the transient behavior of the PV system. Moreover, the suggested DC-link controller removes the DC offsets, which appear in case of gradient increase or decrease in the input PV power. In contrast to the conventional PI controller, which has poor performance at such circumstances. The active and reactive power exchange with the grid is managed using a computationally efficient finite-set model predictive control (FS-MPC) algorithm. Furthermore, switching frequency minimization is added as a secondary objective using a weighting factorless procedure. The grid-voltage sensors are eliminated and estimated using an extended Kalman filter (EKF). The overall control strategy is evaluated using experimental implementation, hardware-in-the-loop (HIL), and matlab/simulink.

**INDEX TERMS** PV systems, model-based MPPT, irradiance estimation, adaptive DC-link control, FS-MPC, weighting factorless, sensorless control, EKF.

## I. INTRODUCTION

Photovoltaic (PV) energy systems can be adopted for small-scale (power) or large-scale applications [1]. Big merit is the exploitation of the PV energy for isolated loads such as

The associate editor coordinating the review of this manuscript and approving it for publication was Xiaofeng Yang<sup>1</sup>.

irrigation systems in remote areas [2]. Furthermore, PV systems are integrated into the grid using different configuration of power electronics converters. However, the main classification of the PV systems is the single-stage and two-stage grid-connected topologies [3]. The two-stage system is commonly utilized due to the simplicity of its control, especially when considering multi-mode power operation

(in addition to the MPPT) for the PV system [4]. Originally, the maximum power point tracking (MPPT) function is implemented in the DC-DC converter stage (the first stage), and the active and reactive power control are achieved in the DC-AC inverter stage (the second stage). However, other control objectives can be imposed in the two stages to accomplish developments in the grid codes and power quality issues [5].

MPPT is a rich research area, where several methods have been investigated in the literature [6], [7]. Nevertheless, the most commonly utilized methods are the perturb and observe (P&O), and the incremental conductance (INC) [8], [9]. These methods suffer from oscillations around the maximum power point (MPP) and poor performance at fast changing atmospheric conditions [10], [11]. Thus, numerous efforts have been conducted to enhance their behavior [12]. Model-based MPPT algorithms are also discussed in the literature, such as the fractional open-circuit voltage method, and fractional short-circuit current [13]. In this regard, online estimation for the open-circuit voltage or the short-circuit current can be implemented to decrease the power loss in the conventional methods [14]. Furthermore, hybrid techniques, where a combination of two methods can be utilized. For example, a fuzzy logic controller or neural network can be integrated with the P&O method [15], [16]. Recently, and in addition to the MPPT operation of the PV system, grid codes are modified to guarantee grid stability and resilience. For instant, constant power generation (CPG) is a modern regulation for PV systems, where the produced PV power is limited if it exceeds a certain threshold [5], [17].

Various attempts have been proposed to enhance the performance of the MPPT. Current-based perturbation algorithm with variable perturbation is presented in [18], where the range of the operating current is adaptively modified at step change of irradiance. However, an expensive irradiance sensor is added to detect the change in the irradiance. In [19], a modified P&O with online open-circuit voltage estimation is suggested, where the P-V characteristic is divided into four sectors. The far sectors form the MPP utilize a large voltage step-size and the other two sectors use a smaller one. Similarly, an irradiance sensor is required to identify the sectors. Furthermore, only simulation results are given in this work. In [10], an additional current check ( $\Delta i$ ) condition is added to the conventional P&O method to improve its performance at fast varying irradiance conditions. However, the system is tested using simple profiles for the PV power variation. Several modifications have been suggested for the P&O technique in [20], based on the observation that the MPP location is restricted to a certain region under irradiance change. However, this method does not account for the wide range variation of the MPP when the temperature varies. A hybrid technique between the open-circuit method and the P&O is presented in [21]. At fast changing atmospheric conditions, this method suffers from remarkable power loss as the case of the conventional fractional open-circuit method. An online estimation technique for the open-circuit voltage is given in [22]. Major concern is the tuning of the

proportionality factor between the open-circuit voltage and the MPP at different operating conditions. FS-MPC is combined with the model of the PV source in [23] to enhance the performance of the P&O. In this technique, several constants are required to model the characteristics of the PV source. Furthermore, high computation burden and dependency on the utilized converter are the major drawbacks of this method. Multiple-power-sample implementation approach for the P&O method is conducted in [24], to differentiate between the power change due to step-size perturbation and the power change due to dynamic change of the PV power. The methodology suffers from slow start-up behavior. Furthermore, it assumes that the variation of the irradiance is linear, which is not accurate in real atmospheric conditions.

PV model-based MPPT approaches have a very good tracking behavior [25], especially when considering variable atmospheric conditions, due to the restriction imposed on the developed PV model. A temperature-based algorithm is provided in [26], which limits the reference voltage according to the temperature variation. It is considered an efficient technique when the arrangement of the PV array configuration guarantees that the effect of the irradiance change on the MPP voltage is minor. Therefore, it is suitable for low power PV applications. Curve fitting approach is suggested in [27] to allocate the MPPs. Thus, it suffers from approximations and tuning of some constants for better curve adjustment. Different scenarios for the MPP voltage calculation are considered in [28] to account for the temperature and irradiance change. However, different factors are in need to be calibrated in addition to the utilization of a high-cost irradiance sensor. To this end, Table 1 gives an overview of the MPPT techniques discussed in the literature, which can be simply classified into traditional methods, model-based algorithms, modern techniques, and optimization methods.

Considering this, and according to the literature summary in Table 1, the model-based MPPT techniques have fast transient behavior. However, the utilized models in most of the research in this area are simple to extract the maximum power at various atmospheric conditions. Furthermore, some methods neglect the irradiance effect and other methods neglect the temperature effect. Moreover, additional components are required for implementation in some techniques. Therefore, it is clear that no straightforward or sophisticated method specifies the coordinates of the MPPs, which motivates the authors to conduct the present work. Thus, in this study, the authors provide a new formulation as a locus for the MPPs. The proposed formulation is derived step by step, and the variation of the temperature and irradiance are considered. The expensive irradiance sensor is eliminated and the irradiance is estimated mathematically. Furthermore, the DC-link voltage suffers from undesirable DC offsets due to the gradual or dynamic change of the power at the PV-side. To the best of authors' knowledge, this observation is not addressed before in the two-stage PV system except for [29] (previous publication of the authors). However, only simulation results are provided there. Therefore, an adaptive DC-link controller is

TABLE 1. Comparative summary among the MPPT methods available in the literature.

Remarks	Conventional methods	Model-based algorithms	Modern and intelligent approaches	Optimization techniques
Techniques	The most common techniques in this group are the P&O and INC method [8]. Basically, the working principle of such methods is inspired by the characteristics of the PV source. Other modified and improved versions of P&O or INC [10], [20], [30]–[32] also belong to this category.	The model-based strategies seek a determination for the location of the MPP. Commonly, the fractional open-circuit method and fractional short-circuit current are employed in this classification [21].	Fuzzy logic controller and artificial neural network are candidates for implementation in this set [33]. Furthermore, model predictive control, where a cost function is used to select the optimal switching state [34].	Several optimization methods have been discussed in the literature [35]. Furthermore, continuous development of such methods is still ongoing. For example, particle swarm optimization, ant colony, bat algorithm, and simulated annealing, etc are employed for maximum power harnessing [36], [37].
Merits	Simple in implementation and structure. Furthermore, the dependency on the system’s parameter diminishes in this group. Low-cost execution platform is also a big merit of such schemes [38].	Simple and easy to perform. Fast response and clear principle.	Enhanced steady-state response and fast transients are the potential benefits of such approaches.	Able to capture the maximum power in case of partial shading conditions. Limited power oscillation during steady-state operation.
Drawbacks	Poor steady-state behavior, slow transient response, and inaccurate operation in case of fast-changing atmospheric conditions are considered the major drawbacks of these methods.	Needs an accurate model for the utilized PV source. Some parameters need tuning. Furthermore, some methods require additional components for implementation (to accomplish the open-circuit voltage or short-circuit current measurement).	Need training and tuning efforts. The dependency on parameters of the PV system may affect the robustness of the procedure.	Parameters tuning and complex algorithms are considered the most significant issues related to these methods. Furthermore, the need for a powerful controller increases the system cost.

suggested to solve this problem. Moreover, an extended Kalman filter (EKF) is employed to estimate the grid voltage; thus, grid voltage sensors elimination is accomplished. In brief, the current study proposes an improved control strategy not only for the MPPT operation but also the inverter control is optimized with sensor reduction, which in turn enhances the system’s reliability and reduces the cost. The main outcome and contributions of this research can be summarized as follows:

- A new MPPT technique, which is based on the model of the PV source is suggested. The technique develops a new formulation for the location of the MPPs. Furthermore, CPG algorithm is integrated with the MPPT as a secondary objective without any need for external devices (storage elements). The high-cost irradiance sensor related to the model-based MPPT techniques is eliminated using simple irradiance estimation approaches.
- A new adaptive DC-link controller is proposed to solve the problem of DC-offsets, which happens when the PV power changes dynamically. The suggested controller is considered an effective solution to the poor behavior of the conventional PI controller. Moreover, it enhances the transient of the injected currents.
- A computationally efficient FS-MPC technique is offered to accomplish the active and reactive power exchange with the grid. Additionally, a weighting factorless approach is utilized to minimize the switching frequency of the DC/AC inverter stage.

- All the grid voltage sensors are eliminated and estimated based on an EKF, which is considered an effective backup strategy.

The remainder of this paper is organized as follows: The model of the two-stage PV system is briefly discussed in Sec. II. The proposed model-based MPPT strategy with irradiance estimation is investigated in Sec. III. The adaptive DC-link controller and the computationally efficient FS-MPC is described in Sec. IV. The results and discussion are given in Sec. V. Sec. VI provides the future scope and some key points. Finally, remarks and outcome of the paper are concluded in Sec. VII.

II. THE MODEL OF THE TWO-STAGE PV TOPOLOGY

The two-stage PV system consists of a PV source, boost converter, two-level inversion stage, and filter for grid integration. The model of the PV source will be investigated in the following section, where the proposed MPPT method is based on that model. The boost converter can be simply described by two states of operation related to the action of its switch. The benefit of that converter is to enable the MPPT function in the PV system [3]. The inverter stage with grid connection is shown in Fig. 1. The behavior of this part from the PV system can be formulated as

$$v_{abc} = u_{abc} + L_f \frac{di_{abc}}{dt} + R_f i_{abc}, \tag{1}$$

where  $v_{abc}$  are the three-phase voltages of the grid,  $i_{abc}$  are the line currents,  $u_{abc}$  are the inverter output voltages,

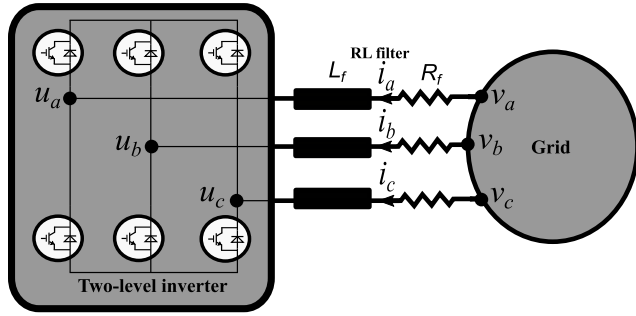


FIGURE 1. The configuration of the grid-connected PV inverter.

and  $L_f$  and  $R_f$  are the filter parameters (inductance and resistance).

In the rotating reference frame ( $d-q$ ), Equation (1) is restructured as

$$v_d = u_d + L_f \frac{di_d}{dt} + R_f i_d - \omega L_f i_q, \quad (2)$$

$$v_q = u_q + L_f \frac{di_q}{dt} + R_f i_q + \omega L_f i_d, \quad (3)$$

where  $\omega$  is the angular frequency of the grid. Furthermore, the active and reactive power values in the same frame are

$$P = \frac{3}{2}(v_d i_d + v_q i_q), \quad (4)$$

$$Q = \frac{3}{2}(v_q i_d - v_d i_q). \quad (5)$$

### III. THE PROPOSED MPPT STRATEGY FOR THE TWO-STAGE PV SYSTEM

#### A. PV MODEL-BASED MPPT ALGORITHM WITH CONSTANT POWER GENERATION

In this section, the effect of both temperature and irradiance on the MPP voltage is investigated, where an accurate formulation is chased. In this regard, the analysis is firstly explored at the open-circuit point and then transferred to the MPP. The open-circuit point is intentionally used for this purpose because of the simplicity of calculation at this point. According to the single-diode model of the PV source, the current-voltage (I-V) relation is given by [39], [40]

$$i_{pv} = i_{ph} - i_s [e^{\frac{v_{pv} + i_{pv} R_s}{n N_s v_{th}}} - 1] - \frac{v_{pv} + i_{pv} R_s}{R_p}, \quad (6)$$

where  $i_{ph}$  is the photovoltaic current,  $n$  is the diode ideality factor,  $i_s$  is the saturation current of the diode,  $R_s$  is the module series resistance,  $R_p$  is the module shunt resistance,  $v_{th}$  is the thermal voltage,  $N_s$  is the number of series cells in the module,  $i_{pv}$  is the delivered PV current, and  $v_{pv}$  is the output PV voltage.

At first, the irradiance effect at open-circuit condition ( $i_{pv} = 0, v_{pv} = v_{oc}$ ) is examined, where the response of the PV generator (Equation (6)) can be estimated as

$$0 = i_{ph} - i_s [e^{\frac{v_{oc}}{n N_s v_{th}}} - 1] - \frac{v_{oc}}{R_p}. \quad (7)$$

Ordinarily, the shunt resistance ( $R_p$ ) is high; thus, the current passing through this branch is neglected. Therefore, (7) can be further simplified to

$$i_{ph} = i_s [e^{\frac{v_{oc}}{n N_s v_{th}}} - 1]. \quad (8)$$

Solving (8) for  $v_{oc}$ , one can get

$$v_{oc} = n N_s v_{th} \ln\left(\frac{i_{ph} + i_s}{i_s}\right). \quad (9)$$

The diode saturation current  $i_s$  (in the numerator) can be neglected with respect to  $i_{ph}$ ; thus, (9) can be put in the following form

$$v_{oc} = n N_s v_{th} \ln\left(\frac{i_{ph}}{i_s}\right). \quad (10)$$

The previous formula is correct at the standard test condition (STC), *i.e.*, 25°C, and 1000 W/m<sup>2</sup>. To this point, the irradiance effect is considered, *i.e.*, temperature is constant. Similarly, taking additional operating point, another formula can be written

$$v_{ocu} = n N_s v_{th} \ln\left(\frac{i_{phu}}{i_s}\right), \quad (11)$$

where  $v_{ocu}$  is the open-circuit voltage at the new point (new irradiance condition), and  $i_{phu}$  is updated photovoltaic current. Subtracting (10) from (11), the old open-circuit voltage (at STC) in comparison with the new one can be derived as

$$v_{ocu} = v_{oc} + n N_s v_{th} \left[ \ln\left(\frac{i_{phu}}{i_{ph}}\right) \right]. \quad (12)$$

The photovoltaic current is proportional to the irradiance level ( $G$ ); thus, exchanging the currents with the irradiance gives

$$v_{ocu} = v_{oc} + n N_s v_{th} \left[ \ln\left(\frac{G_b}{G_a}\right) \right], \quad (13)$$

where  $G_a$  is the irradiance at STC, and  $G_b$  is the new irradiance. Fig. 2 shows the power-voltage (P-V) characteristics of the PV source (KC200GT module) at numerous irradiance conditions. One can observe that the spacing among the open-circuit points at high irradiance levels is small. However, it increases as the irradiance value decreases, which represents a logarithmic relationship.

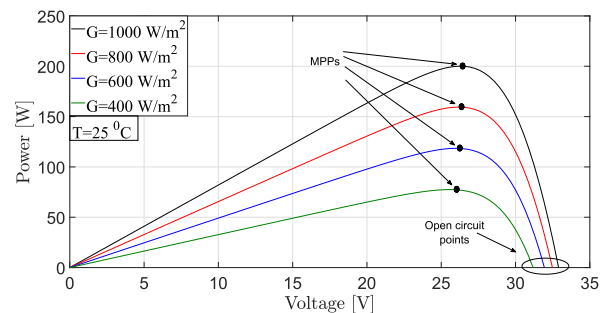


FIGURE 2. P-V characteristics at various irradiance levels.

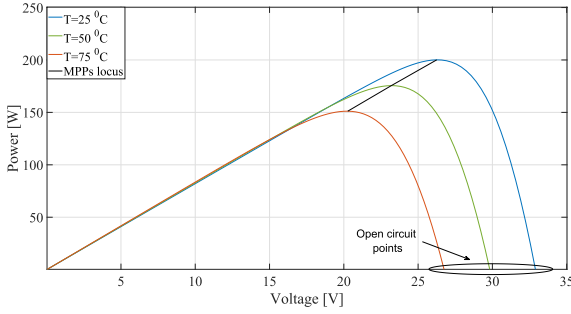


FIGURE 3. P-V characteristics at various temperature conditions.

Considering the above notice, it is quite obvious that the spacing among the MPPs is similar to the open-circuit points. However, the drop (decline) manner of the MPPs is smaller than the open-circuit ones; thus, the natural logarithm (to the base  $e$ ) in (13) is replaced with the common one (to the base 10) to have an accurate estimation for the locus of the MPPs. This results in the following expression

$$v_{mu} = v_{mn} + nN_s v_{th} \left[ \log\left(\frac{G_b}{G_a}\right) \right], \quad (14)$$

where  $v_{mu}$  is the new MPP voltage at a definite irradiance value, and  $v_{mn}$  is the MPP voltage at STC.

Secondly, the temperature effect is examined. Fig. 3 shows the P-V curve at numerous temperature values, where the relation between the open-circuit voltages and the temperature is simply linear. The same perception applies to the MPP voltages; thus,

$$v_{mt} = v_{mn} + k_v(T - T_n), \quad (15)$$

where  $v_{mt}$  is the updated MPP voltage due to temperature variation,  $k_v$  is the open-circuit voltage temperature constant, and  $T_0$  is the temperature at STC. To this end, combining (14) and (15), to get the whole effect of the atmospheric conditions (irradiance and temperature) on the MPP voltage, the following can be obtained

$$v_{ml} = v_{mn} + nN_s v_{th} \left[ \log\left(\frac{G_b}{G_a}\right) \right] + k_v(T - T_0), \quad (16)$$

where  $v_{ml}$  is the location of MPP voltages at any atmospheric condition. Further manipulation can be subjected to (16)

$$v_{ml} = v_{mn} \left[ 1 + \frac{nN_s v_{th}}{v_{mn}} \left[ \log\left(\frac{G_b}{G_a}\right) \right] \right] + k_v(T - T_0), \quad (17)$$

$$v_{ml} = v_{mn} \left[ 1 + k \log\left(\frac{G_b}{G_a}\right) \right] + k_v(T - T_0), \quad (18)$$

where  $k = nN_s v_{th}/v_{mn}$ .

To this end, the constant power generation (CPG) algorithm is activated if the PV input power ( $p_{pv}$ ) exceeds a certain predefined value ( $p_{ref}$ ). Normally, this value is a fraction of the capacity of the installed PV system. The transition between the MPPT mode and the CPG mode can be simply

described by

$$Mode \equiv \begin{cases} \text{MPPT}, & \text{if } p_{pv} \leq p_{ref}, \\ \text{CPG}, & \text{if } p_{pv} > p_{ref}. \end{cases} \quad (19)$$

## B. IRRADIANCE ESTIMATION

According to (18), the MPP voltage locus as a function of the atmospheric conditions ( $G, T$ ) is specified. Thus, to calculate the MPP voltage, the irradiance and temperature should be known. To reduce the number of required sensors, the irradiance is estimated using the existing voltage and current sensors. This reduces the system's cost, as the irradiance sensor is expensive [41]. Furthermore, the system reliability will be enhanced.

A simple approach can be implemented to estimate the irradiance with the help of an online estimation for the photovoltaic current or the short-circuit current. Referring to (6), which expresses the I-V relation at any condition, the equation can be rearranged to get the photovoltaic current

$$i_{ph} = i_{pv} + i_s \left[ e^{\left( \frac{v_{pv} + i_{pv} R_s}{nN_s v_{th}} \right)} - 1 \right] + \frac{v_{pv} + i_{pv} R_s}{R_p}. \quad (20)$$

A quite sufficient approximation can be introduced to the previous formula by replacing the photovoltaic current ( $i_{ph}$ ) with the short-circuit current ( $i_{sc}$ ), which results in

$$i_{sc} = i_{pv} + i_s \left[ e^{\left( \frac{v_{pv} + i_{pv} R_s}{nN_s v_{th}} \right)} - 1 \right] + \frac{v_{pv} + i_{pv} R_s}{R_p}. \quad (21)$$

It is worth mentioning that different formulations for the diode saturation current are given in the literature [42], [43]. Therefore, the irradiance can be estimated from

$$\hat{G} = \frac{i_{sc}}{i_{scn}} G_0, \quad (22)$$

where  $\hat{G}$  is the estimated irradiance,  $i_{scn}$  is the nominal short-circuit current at STC, and  $G_0 = 1000 \text{ W/m}^2$ .

A second approach can be utilized for irradiance estimation in accordance with the international standard IEC 60891 [40], [44]

$$\hat{G} = G_0 \left[ \frac{i_{scnu} + \Delta i}{i_{scnu} + \frac{k_i}{k_v} (R_s \Delta i + \Delta v)} \right], \quad (23)$$

where  $k_i$  is the short-circuit current temperature coefficient,  $\Delta i$  and  $\Delta v$  are the variation of the PV current and voltage due to the change in atmospheric conditions, and they can be calculated from

$$\Delta i = i_{pv} - i_m, \quad (24)$$

$$\Delta v = v_{pv} - v_m, \quad (25)$$

where  $i_m$  and  $v_m$  are the current and voltage at MPP. These values at STC are available in the data-sheet. However, to consider the variation of conditions, we suggest updating the values of the current and voltage at MPP from

$$i_m = i_{mn} + k_i(T - T_0), \quad (26)$$

$$v_m = v_{mn} + k_v(T - T_0), \quad (27)$$

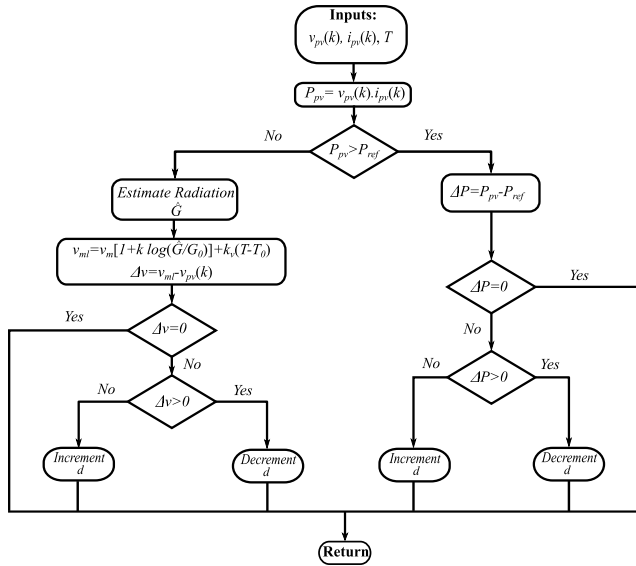


FIGURE 4. The proposed model-based MPPT with constant power generation ability.

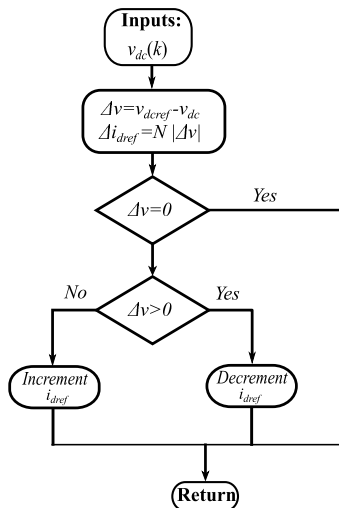


FIGURE 5. The proposed adaptive DC-link controller.

where  $i_{mn}$  is the MPP current at STC. Furthermore, the corrected short-circuit current for irradiance estimation is defined as

$$i_{scnu} = i_{scn} + k_i(T - T_0). \quad (28)$$

The final algorithm for the suggested dual-mode power generation of the two-stage PV system is illustrated in the flowchart shown in Fig. 4.

#### IV. THE PROPOSED FS-MPC APPROACH WITH ENHANCED DC-LINK DYNAMICS

##### A. THE ADAPTIVE DC-LINK VOLTAGE CONTROLLER

Normally, the DC-link between the boost converter and the inverter is controlled using a linear PI controller, which provides the reference current for the inverter's inner current

control loop. As mentioned previously, the behavior of the PI controller under rapidly changing atmospheric conditions is unsatisfactory [45]. Furthermore, it has poor disturbance rejection capability [46]. The DC-link in the two-stage PV system suffers from offsets when a gradual increase or decrease in the PV power happens. This observation is not well-documented in the literature in the area of PV systems. Therefore, a new adaptive DC-link controller is designed in this work to solve this problem. The reference current is calculated according to the difference between the reference voltage and the sensed DC-link one. Furthermore, the step-size is tuned adaptively from

$$\Delta i_{dref} = N |v_{dcref} - v_{dc}|, \quad (29)$$

where  $N$  is an adjustable constant, and  $v_{dcref}$  is the reference value of the DC-link voltage. Fig. 5 shows the updating mechanism of the adaptive DC-link controller.

##### B. COMPUTATIONALLY EFFICIENT FS-MPC WITH WEIGHTING FACTORLESS PROCEDURE

The FS-MPC principle depends on the discrete-time model of the system; thus, applying Euler method for discretization in the  $d$ - $q$  reference frame (Equations (2) and (3)), one obtains

$$i_d(k+1) = \left(1 - \frac{T_s R_f}{L_f}\right) i_d(k) + \omega T_s i_q + \frac{T_s}{L_f} (v_d(k) - u_d(k)), \quad (30)$$

$$i_q(k+1) = \left(1 - \frac{T_s R_f}{L_f}\right) i_q(k) - \omega T_s i_d + \frac{T_s}{L_f} (v_q(k) - u_q(k)), \quad (31)$$

where  $T_s$  is the sampling period. The two-level inverter has 8 switching vectors; and hence, according to the cost function design, the best one will be selected. FS-MPC adds flexibility to the design of the cost function; thus, in this work the switching frequency minimization is added as a secondary control objective. Conventionally, a weighting factor is used as a compromise between the main objective and the secondary one. Therefore, the two objectives can be implemented according to one control law (cost function) as

$$g = |i_d(k+1) - i_{dref}(k+1)| + |i_q(k+1) - i_{qref}(k+1)| + \lambda \sum_{i=1}^8 |S_i(k) - S(k-1)|, \quad (32)$$

where  $S(k)$  is the present switching instant,  $S(k-1)$  is the previous one, and  $\lambda$  is a weighting factor. The predicted reference currents can be evaluated using linear extrapolation as

$$i_{dref}(k+1) = 2 i_{dref}(k) - i_{dref}(k-1), \quad (33)$$

$$i_{qref}(k+1) = 2 i_{qref}(k) - i_{qref}(k-1). \quad (34)$$

To reduce the computational burden of the conventional FS-MPC (8 iterations), the reference voltage vector (RVV) is directly calculated in the proposed FS-MPC. This can be accomplished by substituting  $i_{dref}(k+1)$  and  $i_{qref}(k+1)$

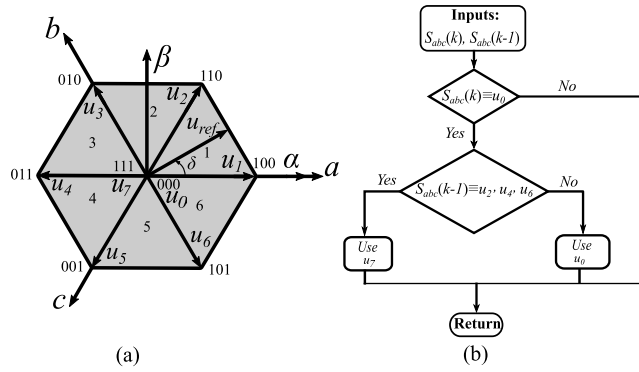


**FIGURE 6. (a) Sectors distribution of the two-level inverter. (b) Switching frequency minimization based weighting factorless technique.**

instead of  $i_d(k+1)$  and  $i_q(k+1)$  in (30) and (31), which gives

$$u_{dref}(k) = R_f i_d(k) - \frac{L_f}{T_s} (i_{dref}(k+1) - i_d(k)) + \omega L_f i_q + v_d(k), \quad (35)$$

$$u_{qref}(k) = R_f i_q(k) - \frac{L_f}{T_s} (i_{qref}(k+1) - i_q(k)) - \omega L_f i_d + v_q(k). \quad (36)$$

Then, the RVV in the  $\alpha$ - $\beta$  reference frame is obtained as (using Park transformation)

$$u_{\alpha\beta ref}(k) = \begin{bmatrix} \cos(\theta) & \sin(\theta) \\ -\sin(\theta) & \cos(\theta) \end{bmatrix} u_{dqref}(k). \quad (37)$$

As a result the position (sector) of the reference voltage in the  $\alpha$ - $\beta$  frame is computed from

$$\delta(k) = \text{atan2}(u_{\beta ref}(k), u_{\alpha ref}(k)). \quad (38)$$

Therefore, the cost function subjected to minimization is modified to

$$g_m = |u_{\alpha}(k) - u_{\alpha ref}(k)| + |u_{\beta}(k) - u_{\beta ref}(k)|, \quad (39)$$

where  $u_{\alpha}(k)$  and  $u_{\beta}(k)$  are the voltage vectors in a certain sector and adjacent to the RVV ( $u_{ref}$ ) specified according to (38) (see Fig. 6). According to this design of cost function, only three calculation of the cost function are required to get the optimal switching vector. For example, if the selected sector is sector one, the two voltage vectors 100 and 110 along with one of the zero voltage vectors (000 or 111) are evaluated in the cost function.

The weighting factor in the conventional FS-MPC (Equation (32)) is eliminated to save the efforts of tuning. Thus, and as there are two zero voltage vectors in the two-level configuration (000 or 111), one of them is selected to be applied according to the cost function design. To be specific, the zero voltage vector 000 is selected in the present design. However, if the previous switching state has two ones, *i.e.*, the previous applied voltage vector is one of  $u_2$ ,  $u_4$  or  $u_6$  (see Fig. 6), it is more proper to consider the other zero

voltage vector (111) for application. This reduces the number of commutations, and hence the switching frequency. Fig. 6 shows the proposed algorithm for eliminating the weighting factor to minimize the switching frequency.

### C. GRID-VOLTAGE ESTIMATION BASED ON EKF

The EKF is an efficient estimator and its design is also based on the discrete-time model of the system [3], and hence it fits in the overall design of the FS-MPC idea. So, it is integrated into the PV system to eliminate all the grid-voltage sensors (3 sensors). Detailed explanation of the EKF can be found in [3], [47]. However, briefly, it contains two stages of prediction and correction, and its design is formulated within these two stages. The prediction stage includes the state vector prediction and the covariance matrix error prediction as follows

$$\hat{x}^-(k) = A_d \hat{x}(k-1) + B_d u(k-1). \quad (40)$$

$$P^-(k) = f(k) P(k-1) f(k)^T + Q, \quad (41)$$

where

$$f(k) = \frac{\partial}{\partial x} (A_d x(k) + B_d u(k))|_{\hat{x}^-(k)}, \quad (42)$$

where  $f(k)$  is the partial derivatives of the state vector elements with respect to each others.

The correction stage is expressed as

$$K(k) = P^-(k) C_d^T (C_d P^-(k) C_d^T + R)^{-1}. \quad (43)$$

$$\hat{x}(k) = \hat{x}^-(k) + K(k) (y(k) - C_d \hat{x}^-(k)). \quad (44)$$

$$P(k) = P^-(k) - K(k) C_d P^-(k). \quad (45)$$

where  $A_d$ ,  $B_d$ ,  $C_d$ , and  $D_d$  are the discretized system matrices.  $Q$  and  $R$  are the covariance matrices corresponding to system uncertainty and measurement noise, respectively.  $K(k)$  is the Kalman gain, and  $\hat{x}(k)$  and  $\hat{y}(k)$  are the estimated quantities.

The whole system configuration of the two-stage PV system with the proposed control strategy is illustrated in Fig. 7, where the first stage implements the MPPT and CPG algorithm. The second stage is concerned with the active and reactive power control using an efficient FS-MPC algorithm.

## V. EXPERIMENTAL RESULTS AND EVALUATIONS

### A. DESCRIPTION OF THE EXPERIMENTAL SET-UP

The system under consideration consists of a PV emulator, boost converter, two-level inverter, and inductive load. The PV emulator is constructed using a DC source connected to a branch of two parallel resistors [48]. Firstly, the DC source is connected in series with one resistor to emulate the P-V curve at a certain power level. After a certain interval, another resistor is connected in parallel to the first one to emulate a sudden increase in the power (irradiance). Finally, the added resistor is removed to simulate an abrupt decrease in the output power of the emulator. This is considered an effective and low-cost PV emulator, which does not affect the behavior of the implemented MPPT methods. The output of the PV emulator is connected to the boost converter, which feeds the power to the two-level inverter. Isolated voltage

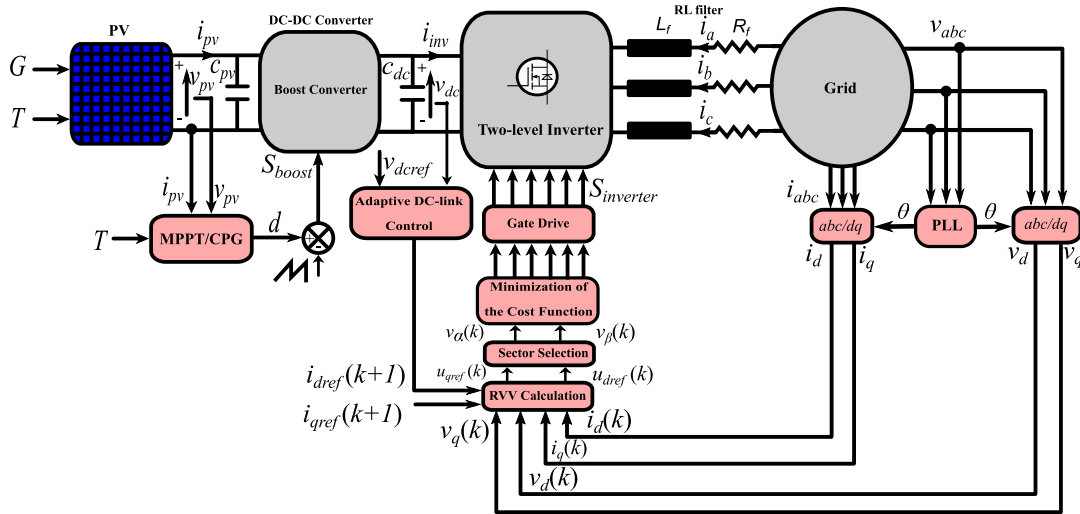


FIGURE 7. The proposed control strategy for the two-stage PV system.

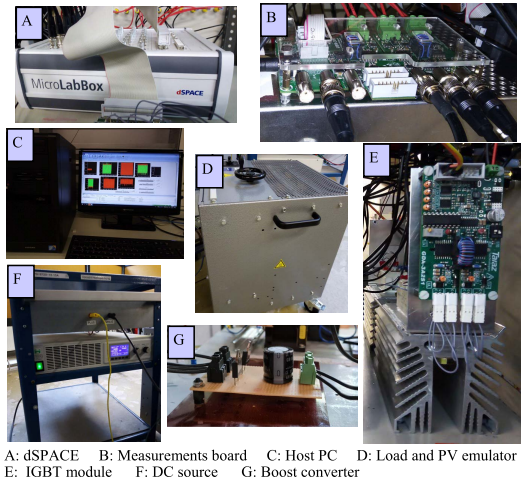


FIGURE 8. Experimental set-up of the two-stage PV system.

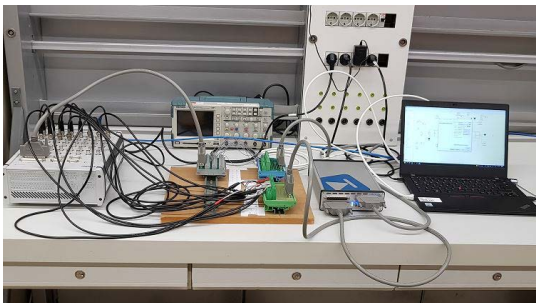


FIGURE 9. The HIL configuration of the PV system.

and current sensing module (USM-3IV) is used to measure the voltages and currents. These measurements are fed to a dSPACE DS1202 MicroLabBox, which is used as a real-time system. The control algorithm is developed using matlab software, and hence the generated switching states are applied

TABLE 2. The parameters of the PV emulation system.

Parameter	Value
Boost inductor ( $L$ )	8.5mH
DC-link capacitance ( $c_{dc}$ )	240 $\mu$ F
Power switch	IGBT-Module FF50R12RT4
Diode ( $D$ )	fast recovery diode BYW77P1200
Switching frequency (boost)	3.33kHz
Load ( $R$ )	5 $\Omega$
Load ( $L$ )	11mH
PV emulator resistors	15 $\Omega$ / 16.5 $\Omega$
DC-link reference voltage ( $v_{dcref}$ )	50V
PV power limit ( $p_{ref}$ )	100W
Sampling time ( $T_s$ )	100 $\mu$ s

to the switches. Smart gate drive module (GDA-2A2S1) is used as interface between the dSPACE controller and the power switches. Furthermore, to evaluate the PV efficiency according to the European standard test [49] (EN50530), hardware-in-the-loop (HIL) is used to build the two-stage grid-connected system. The HIL (RT Box CE) enables the implementation of the PV array and testing of the system under different operating conditions. Figs. 8 and 9 show the experimental and HIL configurations of the PV system, while the specifications and components of the whole PV system are summarized in Table 2.

### B. MPPT AND CPG BEHAVIOR WITH ADAPTIVE DC-LINK CONTROLLER UNDER DIFFERENT IRRADIANCE CONDITIONS

In this subsection, the performance of the MPPT will be investigated, where the instantaneous and average efficiencies are used to assess the behavior of the PV system [11], [20]. Additionally, the European efficiency is calculated for better evaluation and comparison. The static efficiency based on the European scaling factors is given by [23]

$$\eta_{EU} = 0.03 \eta_{05\%} + 0.06 \eta_{10\%} + 0.13 \eta_{20\%} + 0.10 \eta_{30\%} + 0.48 \eta_{50\%} + 0.20 \eta_{100\%}, \quad (46)$$

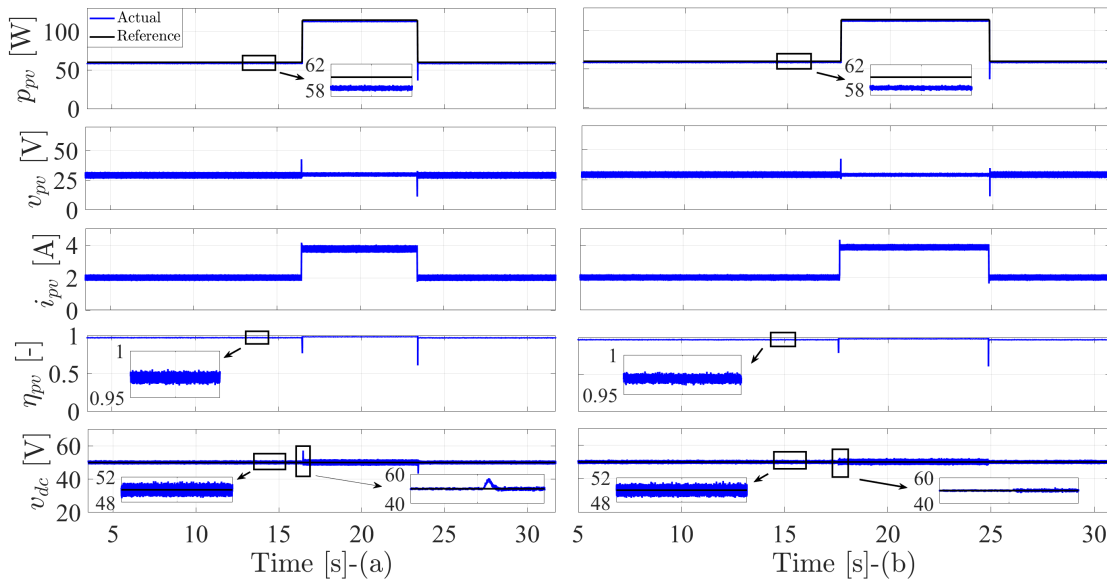


**FIGURE 10.** Performance of the MPPT techniques under step changes of the PV power (experimental): (a) P&O algorithm. (b) PV model-based technique.

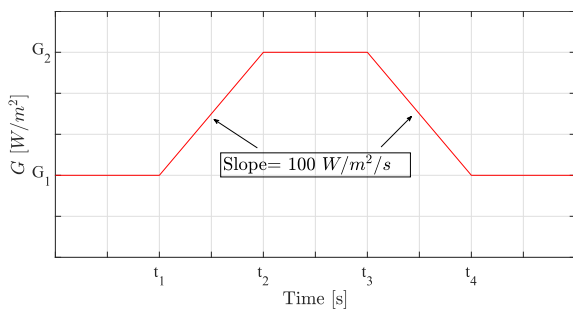


**FIGURE 11.** Ramp profile for efficiency evaluation as recommended by EN50530 test.

where  $\eta_{05\%}$  is the efficiency of the MPPT at 5% of the irradiance. At first, the CPG algorithm is disabled to evaluate the efficiency of the system. The step response of the PV system is implemented experimentally on a down-scaled emulation system. The dynamic behavior of the PV system is conducted using the RT Box CE, where a PV array of 15 kW capacity is considered during implementation. It is worth mentioning that for simulation studies KC200GT PV module is utilized. However, as our proposed MPPT technique is dependent on the model of the PV source, another PV module [50] (BP365) is used for efficiency evaluation to prove the generality of the suggested MPPT technique. Furthermore, an adaptive step [51] (for the conventional and proposed) is included to enhance the steady-state response.

Fig. 10 shows the power, voltage, current, instantaneous efficiency, and the DC-link voltage at step change of the PV power for the P&O and the proposed PV model-based technique, respectively. The PV power ( $p_{pv}$ ) response of the two algorithms is very similar. However, the proposed method

**TABLE 3.** Tracking speed and average efficiency of the MPPT techniques at step change of the PV power.

Method	Tracking speed	$\eta_{pv,avg}(\%)$
P&O	$10 T_s$	97.37
PV model-based	$7 T_s$	97.41

**TABLE 4.** Average efficiency of the MPPT techniques under EN50530 test.

Method	$\eta_{pv,avg}(\%)$
P&O	96.55
Modified P&O	97.87
PV model-based	98.57

has a small improvement in the average PV efficiency. Furthermore, it has a faster tracking speed in comparison with the conventional P&O. Table 3 compares briefly the two methods according to the power response. The PV power exhibits an undershoot at step-down change, which is in correspondence with a high undershoot in the PV voltage ( $v_{pv}$ ). The reason is the fast change of the PV current (inductor current for boost converter), which in turn imposes a negative voltage to resist this fast variation in the current. As a result, the instantaneous efficiency ( $\eta_{pv}$ ) drops to a lower value at the step-down change in comparison with the step-up change of the PV power. The DC-link voltage ( $v_{dc}$ ) with the proposed adaptive technique has a very fast transient behavior, where almost no overshoot or undershoot can be observed. However, for the PI controller, the overshoot and undershoot are approximately 14% and 13.4%, respectively.

It is quite obvious from Table 3, that the improvement in the PV efficiency at step change of the PV power (irradiance) is small; thus, step change is a simple profile to judge the

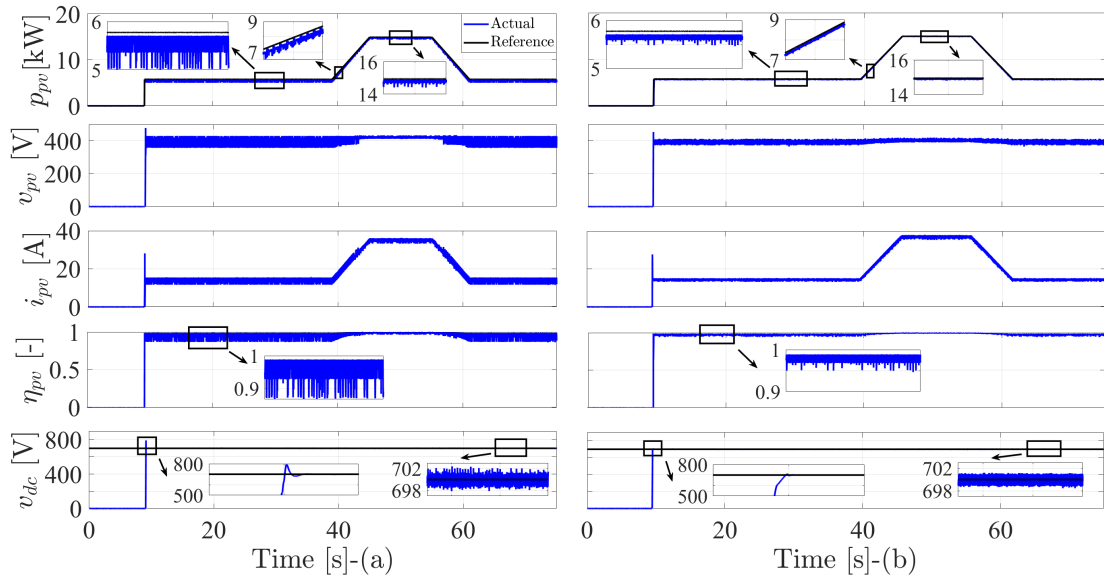


**FIGURE 12. Performance of the MPPT techniques under shortened version of EN50530 test (HIL): (a) P&O algorithm. (b) PV model-based technique.**

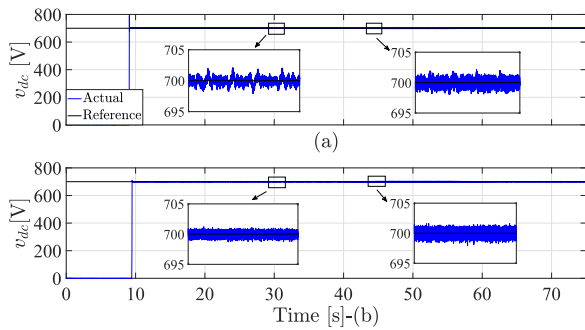


**FIGURE 13. The DC-link voltage behavior with the MPPT techniques under shortened version of EN50530 test (HIL): (a) P&O algorithm. (b) PV model-based technique.**

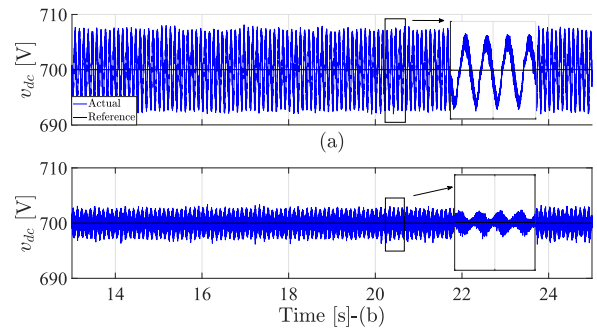


**FIGURE 14. The DC-link voltage behavior under sinusoidal irradiance condition (HIL): (a) PI controller. (b) Adaptive DC-link method.**

**TABLE 5. The efficiency values according to the European scaling factors.**

Method	$\eta_{EU}(\%)$
P&O	97.04
Modified P&O	98.08
PV model-based	98.49

efficiency of the PV system [40]. Therefore, a shortened version of the European standard test [24], [52] is used to evaluate the PV efficiency of the proposed method, which is shown in Fig. 11, where three static periods and two dynamic intervals are included in this test. The test is accomplished using HIL RT Box CE, where a grid-connected PV system is constructed and controlled using the dSPACE real-time system. At this stage, the modified P&O [10] is included for comparison. However, the waveforms are provided for the original P&O and the proposed method. Fig. 12 shows the performance of the P&O and model-based algorithm,

where the power, voltage, current, efficiency, and the DC-link voltage are presented. The PV power oscillations at low irradiance conditions are higher for the P&O method due to the flatness of the P-V curve at these conditions. The instantaneous efficiency at such condition drops to lower than 90%. However, the proposed algorithm efficiency is kept over 95%. Furthermore, the PV power at dynamic weather condition (the rising side of the ramp waveform) is suffering from drift with the P&O. At high irradiance condition, the performance of the P&O is improved, whereas in this case, the change in power due to the perturbation step is more noticeable. Nevertheless, the proposed method oscillations are very tiny. Table 4 summarizes the PV power performance under the standard test, where the average efficiency gain is more than 2% with the proposed MPPT algorithm when compared to the P&O technique. Furthermore, the proposed model-based method has a superior performance in comparison with the modified P&O, where a 0.7% increase in the efficiency is achieved. The European efficiency values for the

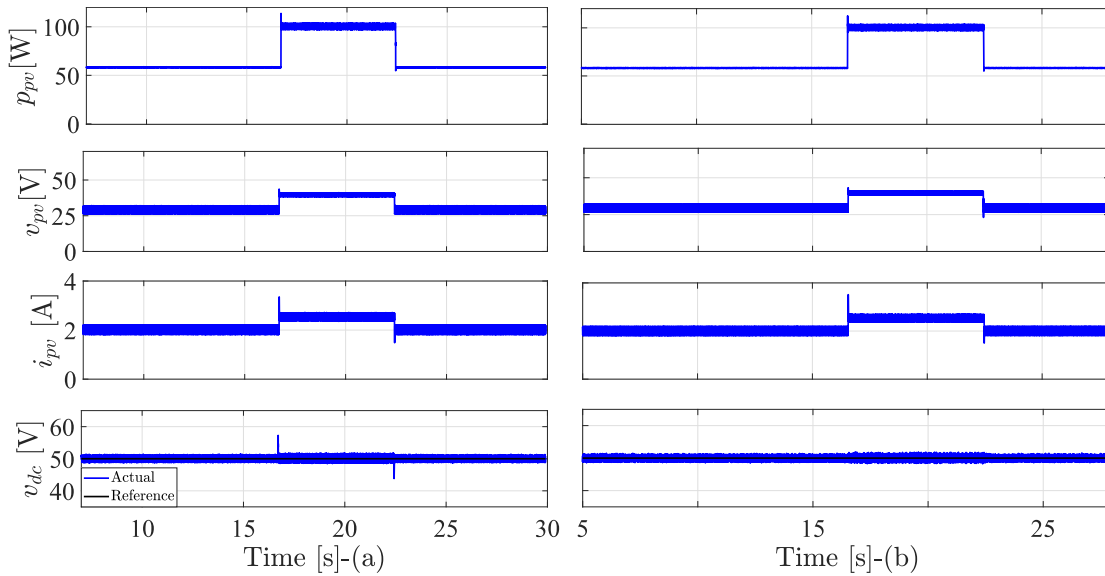


**FIGURE 15. Performance of the two-mode operation of the PV system under step changes of the PV power (experimental): (a) P&O algorithm with CPG. (b) PV model-based technique with CPG.**

traditional P&O, modified P&O, and the proposed method are tabulated in Table 5. The proposed algorithm still has the highest static efficiency value in comparison with the original and modified P&O, where the European efficiency of the proposed method is increased by approximately 1.5% in comparison with the P&O, and 0.4% when compared to the modified one. The DC-link voltage with the proposed adaptive DC-link controller has an enhanced steady-state behavior. This is further investigated in Fig. 13, where some offsets can be seen in the DC-link voltage with the conventional method using PI controller. The reason for this offset is the unsatisfactory performance of the P&O at low irradiance conditions. Additionally, the poor performance of the conventional PI controller at dynamic irradiance variation contributes to these DC offsets. Thus, if the issue of low irradiance is solved, the DC offsets will still exist at dynamic change of the irradiance. Hence, to prove the effectiveness of the proposed adaptive DC-link controller, a sinusoidal profile of the irradiance [11] is used to monitor the variation of the DC-link voltage. Fig. 14 shows the waveform of the DC-link with the PI controller and the adaptive one. It is clear that the behavior of the PI controller is exhibiting DC offsets corresponding to the input PV power variation. The DC offsets have a similar waveform of the variation of the irradiance in case that the MPP is truly tracked. However, the DC-link voltage variation with the adaptive controller is almost negligible.

The performance of the system is further investigated with CPG operation. Fig. 15 presents the behavior of the conventional and the proposed MPPT combined with the CPG algorithm, where an experimental step response is presented. In the first interval, the system is operating in the MPPT mode. When the PV power exceeds the selected limit ( $p_{ref}$ ),

**TABLE 6. Comparison between the conventional and the proposed DC-link controller.**

Parameter	PI	Adaptive method
No. of parameters	2 ( $k_p, k_i$ )	1 ( $N$ )
Implementation	Simple	Simple
Computation burden	Moderate	Low
Performance at step change	Good	Excellent
Tuning efforts	Exists (low)	Very simple
Performance at dynamic conditions	Poor	Excellent

the system operates at CPG condition. It is worth mentioning that the system is operating on the right side of the MPP when the transition happens between the MPPT and the CPG mode. The PV voltages have a similar response with the conventional and the proposed techniques. If the PV currents are compared with the MPPT operation (see Fig. 10), one can observe that the currents have a higher overshoots at CPG operation. As the system is operating at the right side of the P-V curve in this mode (CPG); thus, the current variation (corresponding to small voltage variation) at this side is large. Furthermore, the high undershoot reported in the PV voltage (see Fig. 10) when working under MPPT operation at step-down change of the PV power is decreased. The reason is the decreased value of the PV current at CPG because of the operation at the right side of the P-V characteristics. The DC-link voltage still suffers from overshoots and undershoots at CPG operation due to the fixed gains of the conventional PI controller. However, and thanks to the adaptive step, almost no over or undershoots can be observed at the DC-link voltage of the proposed method. A comparative investigation between the conventional PI controller and the proposed adaptive method is provided in Table 6.

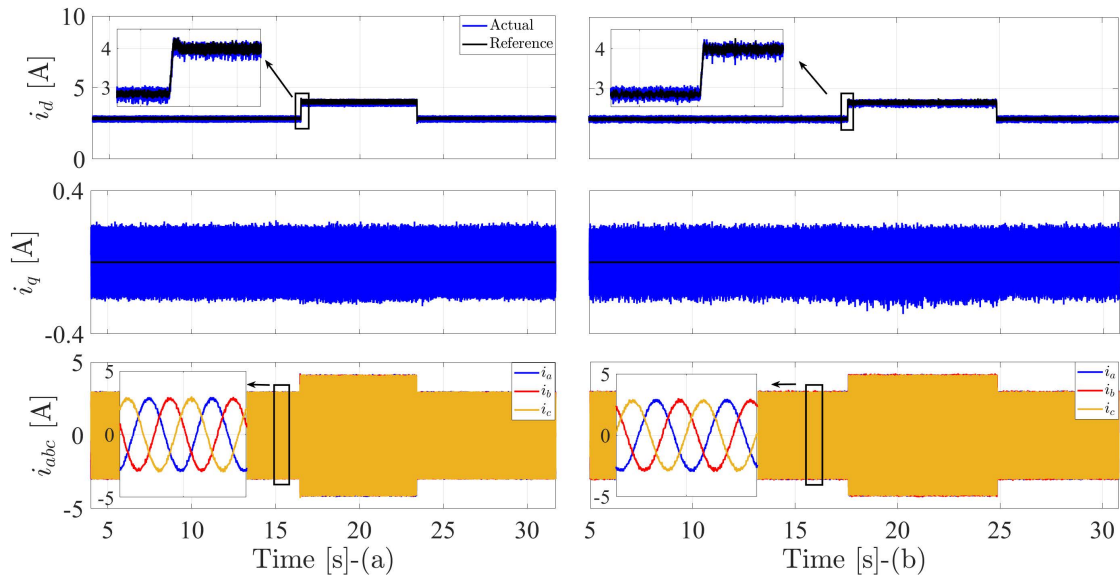


**FIGURE 16.** Performance of inverter control under step change of the PV power (experimental): (a) P&O algorithm with FS-MPC. (b) PV model-based technique with efficient FS-MPC and weighting factorless approach.

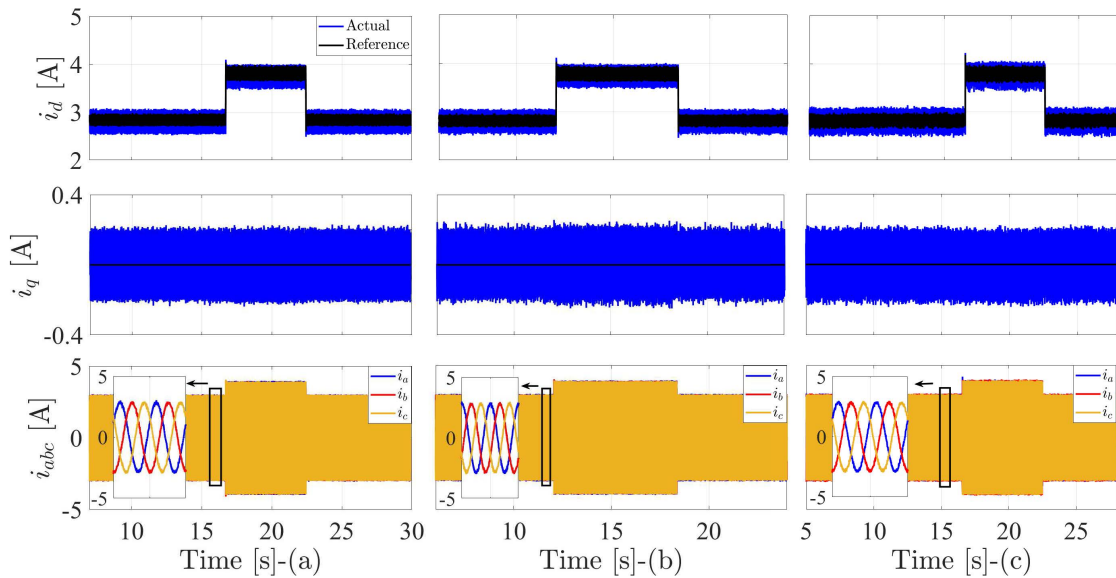


**FIGURE 17.** Performance of inverter control under step change of the PV power (experimental): (a) Two-mode operation (P&O+CPG) with FS-MPC. (b) Two-mode operation (P&O+CPG) with FS-MPC and weighting factor technique. (c) Two-mode operation (PV model-based technique+CPG) with efficient FS-MPC and weighting factorless approach.

**TABLE 7.** THD of the *abc* currents with the conventional and proposed method when the system operating under MPPT.

Method	THD %
Conventional (low/high power)	4.54/ 3.43
Proposed (low/high power)	4.34/ 3.21

**TABLE 8.** Execution time and average switching frequency for inverter control techniques at two-mode power operation.

Method	Execution time ( $\mu s$ )	Avg. $f_s$ (kHz)
Conventional	15.26	2.34
Conventional with weighting	15.20	1.85
Proposed without weighting	12.91	2.06

### C. INVESTIGATION OF THE INVERTER CONTROL USING FS-MPC TECHNIQUES

In this subsection, the performance of the inverter control will be investigated. The conventional FS-MPC, the FS-MPC

with weighting factor for switching frequency minimization, and the proposed efficient FS-MPC with weighting factorless procedure are compared. Firstly, and at MPPT operation, the conventional FS-MPC and the proposed efficient FS-MPC

**TABLE 9. THD of the abc currents with the conventional and proposed method when the system operating under MPPT and CPG.**

Method	THD %
Conventional (MPPT/CPG)	4.54/ 3.43
Conventional with weighting (MPPT/CPG)	4.62/ 3.44
Proposed without weighting (MPPT/CPG)	4.34/ 3.25

**TABLE 10. Summary of steady-state response under EN50530 test for the conventional and the proposed method.**

Method	THD at CPG %	Avg. $f_s$ (kHz)
Conventional	3.93	1.59
Conventional with weighting	4.07	1.32
Proposed without weighting	3.90	1.36

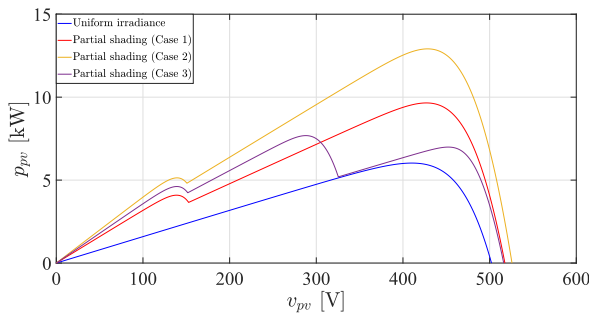


**FIGURE 18. The multiple peak occurrence in case of partial shading in PV system.**

with weighting factorless algorithm are investigated. Fig. 16 shows the direct axis current ( $i_d$ ), the quadrature axis current ( $i_q$ ), and the  $abc$  currents flowing through the inductive load. The  $i_d$  with the proposed algorithm has a fast transient behavior in comparison with the conventional PI controller, where the  $i_d$  with the PI presents a small overshoot inherited from the DC-link dynamics causing a slow transient behavior. The behavior of the  $i_q$  is similar for the two approaches. Table 7 summarizes the THD of the  $abc$  currents for the two techniques, where the THD for the proposed method is better than the conventional one.

Furthermore, the performance of the system when considering CPG operation is examined in Fig. 17. In this case, the conventional FS-MPC, conventional FS-MPC with weighting factor for switching frequency minimization, and proposed efficient FS-MPC without weighting factor are compared. At low power level, the MPPT is enabled and the CPG is activated at high power level. Tables 8 and 9 explore the steady-state response of the three methods, where the proposed method has the lowest execution time in comparison to other methods. The average switching frequency (Avg.  $f_s$ ) with the proposed method is decreased by approximately 12%, and 21% for the conventional with weighting factor. However, the weighting factor procedure comes at the cost of increased THD of the currents. Additionally, efforts for tuning the weighting factor are required. In this regard, at wide range of operation (low to high power or irradiance), the weighting factor procedure is expected to affect the main objective of the controller. Even more, the THD of the injected currents can

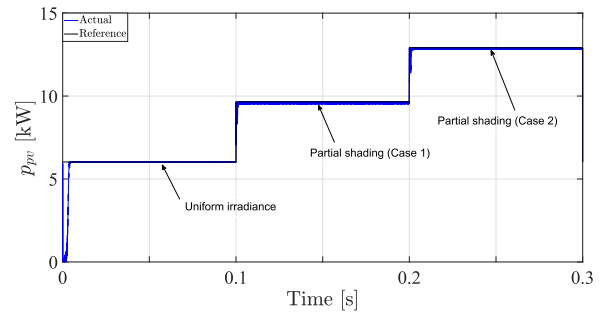


**FIGURE 19. The behavior of the proposed model-based MPPT algorithm at partial shading condition (simulation).**

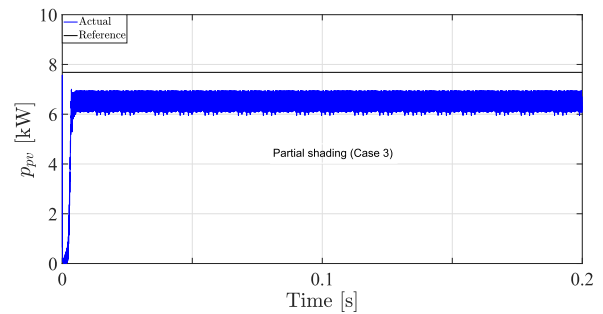


**FIGURE 20. The performance of the proposed model-based MPPT technique at complex partial shading condition (simulation).**

be deteriorated. Thus, online tuning for the weighting factor is mandatory in this case. However, the proposed weighting factorless approach depends on the redundancy states of the converter; thus, a switching state that has the same voltage vector value is selected to reduce the switching frequency resulting in no effect on the THD of the injected currents.

Moreover, the dynamic behavior using HIL is investigated. The results are summarized in Table 10, where the proposed method gives an enhanced THD value of the injected currents. Furthermore, a reduction of 14.5% for the switching frequency is achieved, while the conventional technique with weighting factor gives a 17% reduction.

#### D. PERFORMANCE OF THE PROPOSED MPPT UNDER PARTIAL SHADING CONDITIONS

##### 1) STATIC PARTIAL SHADING CONDITIONS

Normally, the P&O method and the proposed model-based technique are designed for uniform irradiance conditions, where the P-V curve has only one peak under such circumstances. However, partial shading conditions imply the existence of several peaks in the PV characteristics. Therefore, it is expected that the traditional P&O will not be capable of extracting the global maximum all the time. In this regard, the studied methods can successfully track the highest peak if this peak is the last one [14]. This case is clarified in Fig. 18, where the characteristics of the PV array are shown at uniform irradiance condition and three cases of partial shading. Fig. 19 shows the behavior of the model-based MPPT, where the system is tested firstly with a uniform irradiance, then two

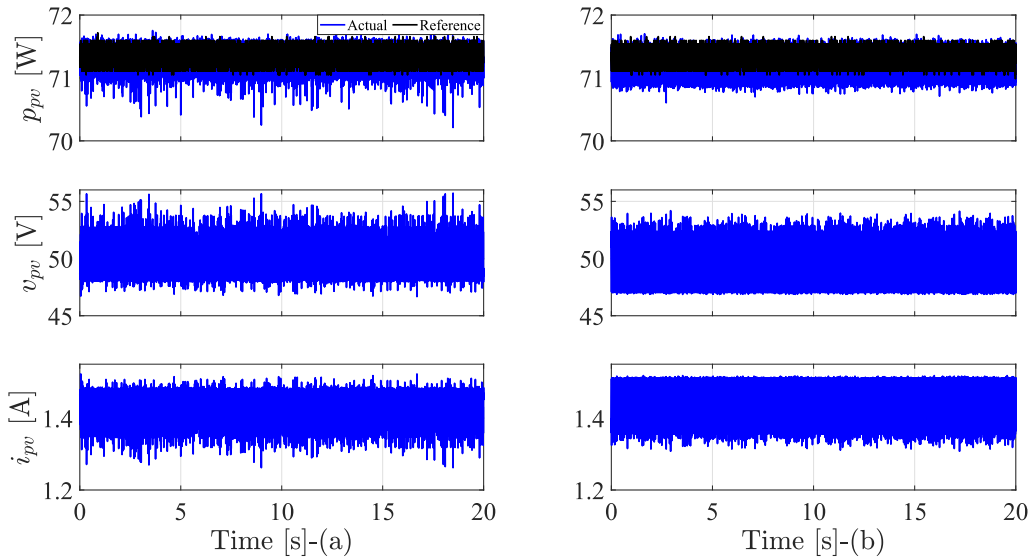


**FIGURE 21. Successful extraction of the maximum power at partial shading condition (HIL): (a) P&O method. (b) PV model-based algorithm.**

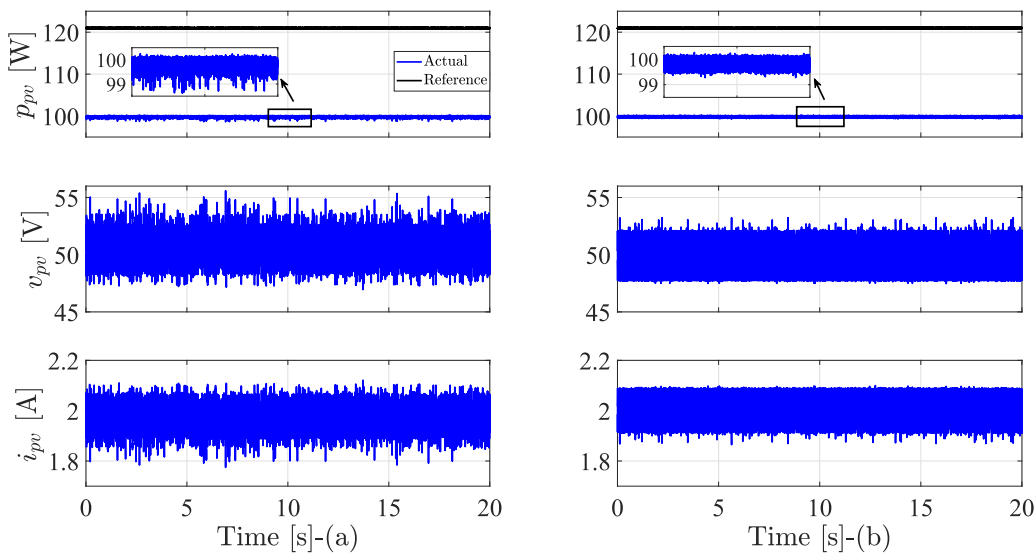


**FIGURE 22. Failure of MPPT to extract the maximum power at partial shading occurrence (HIL): (a) P&O method. (b) PV model-based algorithm.**

successive changes of irradiance occur, which in turn cause the aforementioned cases of partial shading. The proposed MPPT extracts successfully the maximum power in all cases.

Another case is also shown in Fig. 18, where a more challenging partial shading condition is considered. The global peak of this curve occurs in the middle (Case 3). Therefore, the proposed MPPT fails to extract this value. However, still, the behavior of the MPPT technique is reasonable as clarified in Fig. 20, where it sticks to a local peak (the last one).

Further investigation on the performance of the proposed model-based MPPT method using experimental HIL tests is provided. In one case, which is shown in Fig. 21, the traditional P&O and the proposed method have the ability

to extract the maximum power at partial shading. In another case, where the highest peak is not the last one, both methods are trapped at local peak. This is given in Fig. 22. A more complex condition is further investigated for HIL implementation, where the peak is in the middle (see Fig. 18). Fig. 23 shows the performance of the P&O and the proposed technique. Both methods fail to harness this global peak as mentioned previously.

The results show that the proposed method gives the lowest oscillation behavior in all waveforms, especially the power, which greatly enhances the PV efficiency. This further proves the effectiveness of the proposed method in comparison with the conventional P&O. It should be mentioned that the partial

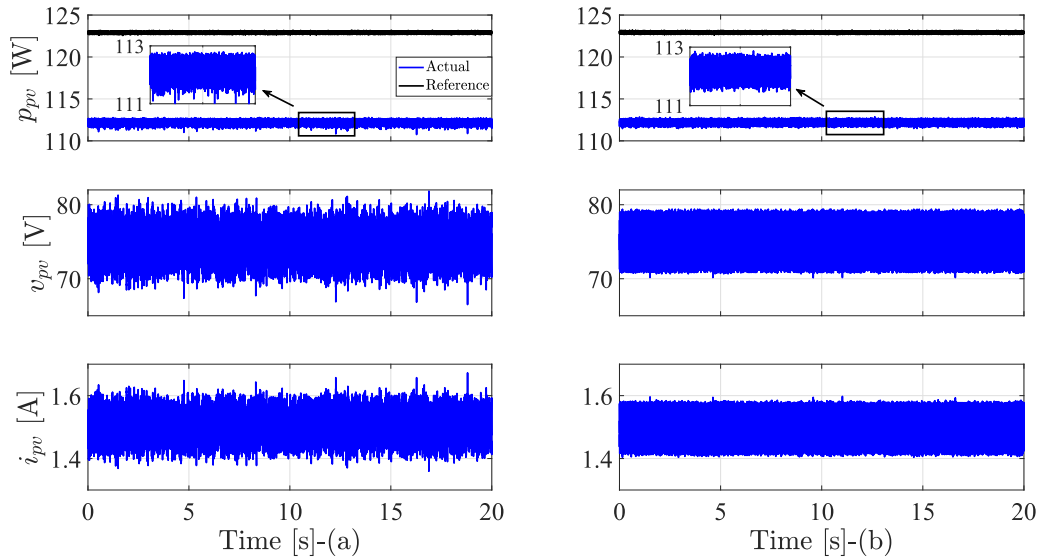


**FIGURE 23. Failure of MPPT to extract the maximum power at complex partial shading condition (HIL): (a) P&O method. (b) PV model-based algorithm.**

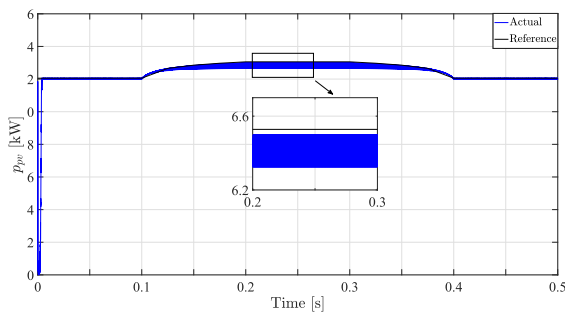


**FIGURE 24. The performance of the proposed MPPT under dynamic partial shading condition (simulation).**

shading cases are studied on a down-scaled PV power system for the experimental HIL implementation.

## 2) DYNAMIC PARTIAL SHADING CONDITIONS

The previously studied conditions consider static partial shading. However, dynamic partial shading is an important issue that should be discussed [53]. A dynamic partial shading profile is studied to further investigate the behavior of the proposed method, where the irradiance is kept constant on part of the system and varied dynamically on the other part. More information on this situation can be found in [53]. Therefore, a similar waveform is chosen, which is shown in Fig. 11 to test the proposed scheme under such condition. Fig. 24 shows the MPPT behavior of the proposed method under dynamic partial shading condition. The results show that the proposed technique fails to follow the dynamic partial shading profile. However, it gives a satisfactory performance. Undoubtedly, further investigations can be performed to test the proposed scheme. Nevertheless, the failure or success rate of the MPPT is considered for future examination.

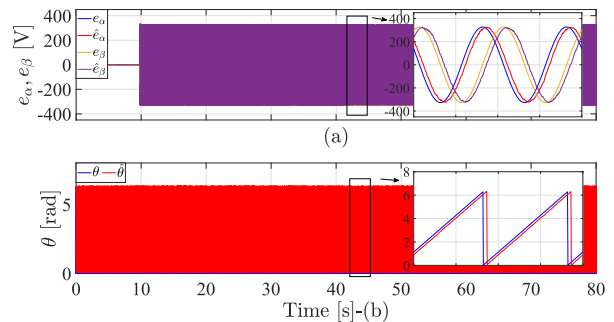


**FIGURE 25. The actual and estimated values under shortened version of EN50530 test using EKF (HIL): (a) Grid-voltage. (b) Grid-angle.**

## E. GRID-VOLTAGE SENSORS ELIMINATION USING EKF

All the voltage sensors are eliminated and estimated online using an EKF. Fig. 25 shows the grid-voltage and angle in the  $\alpha$ - $\beta$  reference frame, where the results show an accurate estimation for the voltages. However, the estimated values are compensated to account for the delay in the digital controller. Furthermore, the execution time of the proposed strategy with EKF is 22.04  $\mu$ s, which represents about 6  $\mu$ s increase with respect to the conventional method.

## VI. FUTURE WORK

A new PV model-based MPPT with the ability to limit the produced PV power is proposed here. However, some points are in need to be discussed to improve the present work and open new directions for future investigations. We summarize this in the following few suggestions:

- Comparative evaluation between the P&O method and the proposed one should be investigated in terms of the success rate for capturing the global peak at different cases. Furthermore, modification of the model-based technique to extract the maximum power in case of partial shading conditions.

- The effect of aging of the PV source is to be fulfilled, and its impact on the model-based method. Furthermore, comparative evaluation for different methods, which use the model of the PV source.
- Investigation of different flexible power control strategies when combined with the proposed MPPT algorithm.
- Irradiance estimation using optimization techniques. In this regard, short-term forecasting for the atmospheric weather conditions can be included for MPPT implementation.
- Sensor reduction, in which the control objective can be effectively implemented or in other cases for effective backup handling situations.
- Online tuning of the weighting factor in the cost function design of the inversion stage. Additionally, adding different control objectives to further optimize the system's performance.
- Robustness assessment and improvement of the FS-MPC, which is used for active and reactive power management.

## VII. CONCLUSION

In this article, a new PV model-based MPPT technique has been presented. The proposed technique is able to switch between the MPPT operation and the CPG. Furthermore, when compared to the conventional P&O method, it gives higher average efficiency (2% increase) according to a shortened version of the EN50530 test. Furthermore, and according to the European scaling factors, the gain in efficiency is increased by 1.5% for the proposed method in comparison with the P&O. The high-cost irradiance sensor is eliminated in our approach. Thus, a reduction in the cost for low-power PV applications can be achieved in addition to enhancing reliability. In the case of partial shading conditions, the behavior of the proposed method is similar to the P&O technique. However, an enhanced steady-state response is obtained with the proposed one. The poor performance of the conventional PI controller at dynamic weather condition is investigated, and the solution using an adaptive DC-link controller is suggested. The presented adaptive DC-link controller provides a fast transient response of the DC-link voltage and the injected currents in comparison with the conventional PI. An efficient FS-MPC approach is utilized for current regulation to further enhance the transient of the inner loop. Moreover, the weighting factor for switching frequency minimization is eliminated, where a reduction by 12% experimentally, and 14.5% using the HIL set-up is accomplished without any effect on the main control objective (current control). Furthermore, the grid voltages are estimated using an EKF, which is considered an effective backup strategy in case of sensor failure.

## REFERENCES

[1] R. Motamarri and N. Bhookya, "JAYA algorithm based on Lévy flight for global MPPT under partial shading in photovoltaic system," *IEEE J. Emerg. Sel. Topics Power Electron.*, vol. 9, no. 4, pp. 4979–4991, Aug. 2021.

[2] M. A. Elgendy, B. Zahawi, and D. J. Atkinson, "Comparison of directly connected and constant voltage controlled photovoltaic pumping systems," *IEEE Trans. Sustain. Energy*, vol. 1, no. 3, pp. 184–192, Oct. 2010.

[3] M. Ahmed, M. Abdelrahem, and R. Kennel, "Highly efficient and robust grid connected photovoltaic system based model predictive control with Kalman filtering capability," *Sustainability*, vol. 12, no. 11, p. 4542, Jun. 2020.

[4] A. Sangwongwanich, Y. Yang, and F. Blaabjerg, "High-performance constant power generation in grid-connected PV systems," *IEEE Trans. Power Electron.*, vol. 31, no. 3, pp. 1822–1825, Mar. 2015.

[5] Q. Peng, A. Sangwongwanich, Y. Yang, and F. Blaabjerg, "Grid-friendly power control for smart photovoltaic systems," *Sol. Energy*, vol. 210, pp. 115–127, Nov. 2020.

[6] T. Ebrahim and P. L. Chapman, "Comparison of photovoltaic array maximum power point tracking techniques," *IEEE Trans. Energy Convers.*, vol. 22, no. 2, pp. 439–449, Jun. 2007.

[7] B. Bendib, H. Belmili, and F. Krim, "A survey of the most used MPPT methods: Conventional and advanced algorithms applied for photovoltaic systems," *Renew. Sustain. Energy Rev.*, vol. 45, pp. 637–648, May 2015.

[8] D. Sera, L. Mathe, T. Kerekes, S. V. Spataru, and R. Teodorescu, "On the perturb-and-observe and incremental conductance MPPT methods for PV systems," *IEEE J. Photovolt.*, vol. 3, no. 3, pp. 1070–1078, Jul. 2013.

[9] H. Rezk, M. Aly, M. Al-Dhaifallah, and M. Shoyama, "Design and hardware implementation of new adaptive fuzzy logic-based MPPT control method for photovoltaic applications," *IEEE Access*, vol. 7, pp. 106427–106438, 2019.

[10] M. Killi and S. Samanta, "Modified perturb and observe MPPT algorithm for drift avoidance in photovoltaic systems," *IEEE Trans. Ind. Electron.*, vol. 62, no. 9, pp. 5549–5559, Sep. 2015.

[11] J. Ahmed and Z. Salam, "An improved perturb and observe (P&O) maximum power point tracking (MPPT) algorithm for higher efficiency," *Appl. Energy*, vol. 150, pp. 97–108, Jul. 2015.

[12] M. A. Elgendy, B. Zahawi, and D. J. Atkinson, "Operating characteristics of the P&O algorithm at high perturbation frequencies for standalone PV systems," *IEEE Trans. Energy Convers.*, vol. 30, no. 1, pp. 189–198, Mar. 2015.

[13] N. Karami, N. Moubayed, and R. Outbib, "General review and classification of different MPPT Techniques," *Renew. Sustain. Energy Rev.*, vol. 68, pp. 1–18, Feb. 2017.

[14] A. Nadeem, H. A. Sher, and A. F. Murtaza, "Online fractional open-circuit voltage maximum output power algorithm for photovoltaic modules," *IET Renew. Power Gener.*, vol. 14, no. 2, pp. 188–198, Feb. 2020.

[15] U. Yilmaz, A. Kircay, and S. Borekci, "PV system fuzzy logic MPPT method and PI control as a charge controller," *Renew. Sustain. Energy Rev.*, vol. 81, pp. 994–1001, Jan. 2018.

[16] S. Messalti, A. Harrag, and A. Loukriz, "A new variable step size neural networks MPPT controller: Review, simulation and hardware implementation," *Renew. Sustain. Energy Rev.*, vol. 68, pp. 221–233, Feb. 2017.

[17] H. D. Tafti, G. Konstantinou, C. D. Townsend, G. G. Farivar, A. Sangwongwanich, Y. Yang, J. Pou, and F. Blaabjerg, "Extended functionalities of photovoltaic systems with flexible power point tracking: Recent advances," *IEEE Trans. Power Electron.*, vol. 35, no. 9, pp. 9342–9356, Sep. 2020.

[18] S. K. Kollimalla and M. K. Mishra, "Variable perturbation size adaptive P&O MPPT algorithm for sudden changes in irradiance," *IEEE Trans. Sustain. Energy*, vol. 5, no. 3, pp. 718–728, Jul. 2014.

[19] A. I. M. Ali and H. R. A. Mohamed, "Improved P&O MPPT algorithm with efficient open-circuit voltage estimation for two-stage grid-integrated PV system under realistic solar radiation," *Int. J. Electr. Power Energy Syst.*, vol. 137, May 2022, Art. no. 107805.

[20] J. Ahmed and Z. Salam, "A modified P&O maximum power point tracking method with reduced steady-state oscillation and improved tracking efficiency," *IEEE Trans. Sustain. Energy*, vol. 7, no. 4, pp. 1506–1515, Oct. 2016.

[21] H. A. Sher, A. F. Murtaza, A. Noman, K. E. Addoweesh, K. Al-Haddad, and M. Chiaberge, "A new sensorless hybrid MPPT algorithm based on fractional short-circuit current measurement and P&O MPPT," *IEEE Trans. Sustain. Energy*, vol. 6, no. 4, pp. 1426–1434, Oct. 2015.

[22] A. Nadeem, H. A. Sher, A. F. Murtaza, and N. Ahmed, "Online current-sensorless estimator for PV open circuit voltage and short circuit current," *Sol. Energy*, vol. 213, pp. 198–210, Jan. 2021.

[23] A. Lashab, D. Sera, and J. M. Guerrero, "A dual-discrete model predictive control-based MPPT for PV systems," *IEEE Trans. Power Electron.*, vol. 34, no. 10, pp. 9686–9697, Oct. 2019.

- [24] H. Abouadane, A. Fakkar, D. Sera, A. Lashab, S. Spataru, and T. Kerekes, "Multiple-power-sample based P&O MPPT for fast-changing irradiance conditions for a simple implementation," *IEEE J. Photovolt.*, vol. 10, no. 5, pp. 1481–1488, Sep. 2020.
- [25] M. A. G. de Brito, L. Galotto, L. P. Sampaio, G. E. de Azevedo e Melo, and C. A. Canesin, "Evaluation of the main MPPT techniques for photovoltaic applications," *IEEE Trans. Ind. Electron.*, vol. 60, no. 3, pp. 1156–1167, Mar. 2013.
- [26] R. F. Coelho, F. M. Concer, and D. C. Martins, "A MPPT approach based on temperature measurements applied in PV systems," in *Proc. IEEE Int. Conf. Sustain. Energy Technol. (ICSET)*, Dec. 2010, pp. 1–6.
- [27] Y.-H. Liu, C.-L. Liu, J.-W. Huang, and J.-H. Chen, "Neural-network-based maximum power point tracking methods for photovoltaic systems operating under fast changing environments," *Sol. Energy*, vol. 89, pp. 42–53, Mar. 2013.
- [28] U. Yilmaz, O. Turksoy, and A. Teke, "Improved MPPT method to increase accuracy and speed in photovoltaic systems under variable atmospheric conditions," *Int. J. Electr. Power Energy Syst.*, vol. 113, pp. 634–651, Dec. 2019.
- [29] M. Ahmed, I. Harbi, R. Kennel, and M. Abdelrahem, "Dual-mode power operation for grid-connected PV systems with adaptive DC-link controller," *Arab. J. Sci. Eng.*, vol. 47, pp. 2893–2907, 2022, doi: 10.1007/s13369-021-05916-w.
- [30] S. M. Sousa, L. S. Gusman, T. A. S. Lopes, H. A. Pereira, and J. M. S. Callegari, "MPPT algorithm in single loop current-mode control applied to DC–DC converters with input current source characteristics," *Int. J. Electr. Power Energy Syst.*, vol. 138, Jun. 2022, Art. no. 107909.
- [31] T. K. Soon and S. Mekhilef, "A fast-converging MPPT technique for photovoltaic system under fast-varying solar irradiation and load resistance," *IEEE Trans. Ind. Informat.*, vol. 11, no. 1, pp. 176–186, Feb. 2014.
- [32] N. E. Zakzouk, M. A. Elshaharty, A. K. Abdelsalam, A. A. Helal, and B. W. Williams, "Improved performance low-cost incremental conductance PV MPPT technique," *IET Renew. Power Gener.*, vol. 10, no. 4, pp. 561–574, Apr. 2016.
- [33] M. N. Ali, K. Mahmoud, M. Lehtonen, and M. M. F. Darwish, "An efficient fuzzy-logic based variable-step incremental conductance MPPT method for grid-connected PV systems," *IEEE Access*, vol. 9, pp. 26420–26430, 2021.
- [34] P. E. Kakosimos and A. G. Kladas, "Implementation of photovoltaic array MPPT through fixed step predictive control technique," *Renew. Energy*, vol. 36, no. 9, pp. 2508–2514, 2011.
- [35] M. Kermadi, Z. Salam, A. M. Eltamaly, J. Ahmed, S. Mekhilef, C. Larbes, and E. M. Berkouk, "Recent developments of MPPT techniques for PV systems under partial shading conditions: A critical review and performance evaluation," *IET Renew. Power Gener.*, vol. 14, no. 17, pp. 3401–3417, Dec. 2020.
- [36] A. M. Eltamaly, "An improved cuckoo search algorithm for maximum power point tracking of photovoltaic systems under partial shading conditions," *Energies*, vol. 14, no. 4, p. 953, Feb. 2021.
- [37] D. Karna, A. Vikram, A. Kumar, and M. Rizwan, "Extraction of maximum electrical power from solar photovoltaic-based grid-tied system," in *Proc. Adv. Energy Technol.* Singapore: Springer, 2022, pp. 351–361.
- [38] P. Manoharan, U. Subramaniam, T. S. Babu, S. Padmanaban, J. B. Holm-Nielsen, M. Mitolo, and S. Ravichandran, "Improved perturb and observation maximum power point tracking technique for solar photovoltaic power generation systems," *IEEE Syst. J.*, vol. 15, no. 2, pp. 3024–3035, Jun. 2020.
- [39] X. Li, Q. Wang, H. Wen, and W. Xiao, "Comprehensive studies on operational principles for maximum power point tracking in photovoltaic systems," *IEEE Access*, vol. 7, pp. 121407–121420, 2019.
- [40] M. Ahmed, M. Abdelrahem, I. Harbi, and R. Kennel, "An adaptive model-based MPPT technique with drift-avoidance for grid-connected PV systems," *Energies*, vol. 13, no. 24, p. 6656, Dec. 2020.
- [41] A. M. Noman, K. E. Addoweesh, and A. I. Alolah, "Simulation and practical implementation of ANFIS-based MPPT method for PV applications using isolated Ćuk converter," *Int. J. Photoenergy*, vol. 2017, pp. 1–15, Dec. 2017.
- [42] M. G. Villalva, J. R. Gazoli, and E. R. Filho, "Comprehensive approach to modeling and simulation of photovoltaic arrays," *IEEE Trans. Power Electron.*, vol. 24, no. 5, pp. 1198–1208, May 2009.
- [43] D. Sera, R. Teodorescu, and P. Rodriguez, "PV panel model based on datasheet values," in *Proc. IEEE Int. Symp. Ind. Electron.*, Jun. 2007, pp. 2392–2396.
- [44] A. Chikh and A. Chandra, "An optimal maximum power point tracking algorithm for PV systems with climatic parameters estimation," *IEEE Trans. Sustain. Energy*, vol. 6, no. 2, pp. 644–652, Apr. 2015.
- [45] R. Kadri, J. P. Gaubert, and G. Champenois, "An improved maximum power point tracking for photovoltaic grid-connected inverter based on voltage-oriented control," *IEEE Trans. Ind. Electron.*, vol. 58, no. 1, pp. 66–75, Jan. 2010.
- [46] M. Ciobotaru, R. Teodorescu, and F. Blaabjerg, "Control of single-stage single-phase PV inverter," *EPE J.*, vol. 16, no. 3, pp. 20–26, Sep. 2006.
- [47] M. Ahmed, M. Abdelrahem, I. Harbi, and R. Kennel, "Sensorless predictive direct power control with on-line inductance estimation for grid-connected PV applications," in *Proc. Eur. Int. Exhib. Conf. Power Electron., Intell. Motion, Renew. Energy Energy Manage. (PCIM)*, 2021, pp. 1–7.
- [48] N. E. Zakzouk, A. K. Abdelsalam, A. A. Helal, and B. W. Williams, "PV single-phase grid-connected converter: DC-link voltage sensorless prospective," *IEEE J. Emerg. Sel. Topics Power Electron.*, vol. 5, no. 1, pp. 526–546, Mar. 2016.
- [49] R. Bründlinger, N. Henze, H. Häberlin, B. Burger, A. Bergmann, and F. Baumgartner, "prEN 50530—The new European standard for performance characterisation of PV inverters," in *Proc. 24th Eur. Photovolt. Sol. Energy Conf.*, Hamburg, Germany, 2009, pp. 3105–3109.
- [50] J. Schönberger, "Modeling a photovoltaic string using PLECS," *Appl. Example*, vol. 13, pp. 1–3, Nov. 2013.
- [51] F. Liu, S. Duan, B. Liu, and Y. Kang, "A variable step size inc MPPT method for PV systems," *IEEE Trans. Ind. Electron.*, vol. 55, no. 7, pp. 2622–2628, Jul. 2008.
- [52] X. Li, H. Wen, Y. Hu, Y. Du, and Y. Yang, "A comparative study on photovoltaic MPPT algorithms under EN50530 dynamic test procedure," *IEEE Trans. Power Electron.*, vol. 36, no. 4, pp. 4153–4168, Apr. 2021.
- [53] M. Chen, S. Ma, J. Wu, and L. Huang, "Analysis of MPPT failure and development of an augmented nonlinear controller for MPPT of photovoltaic systems under partial shading conditions," *Appl. Sci.*, vol. 7, no. 1, p. 95, Jan. 2017.



**MOSTAFA AHMED** (Graduate Student Member, IEEE) was born in Qena, Egypt. He received the B.Sc. (Hons.) and M.Sc. degrees in electrical engineering from Assiut University, Assiut, Egypt, in 2010 and 2015, respectively. He is currently pursuing the Ph.D. degree with the Chair of High-Power Converter Systems (HLU), Technical University of Munich (TUM), Munich, Germany.

He received a Scholarship from the German Academic Exchange Service (DAAD) within the Program "German-Egyptian Research Long Term Scholarship (GERLS)," in 2018, to pursue the Ph.D. degree at the Technical University of Munich. His research interests include renewable energy systems, modeling of photovoltaic systems, MPPT, predictive control of power electronics converters, and sensorless control of photovoltaic systems.



**IBRAHIM HARBI** (Graduate Student Member, IEEE) was born in Beheira, Egypt. He received the B.Sc. (Hons.) and M.Sc. degrees in electrical engineering from Menoufia University, Shebin El-Koum, Egypt, in 2012 and 2016, respectively. He is currently pursuing the Ph.D. degree with the Chair of High-Power Converter Systems (HLU), Technical University of Munich (TUM), Munich, Germany.

He received a Scholarship from the German Academic Exchange Service (DAAD) within the Program "German-Egyptian Research Long Term Scholarship (GERLS)," in 2018, to pursue the Ph.D. degree at the Technical University of Munich. His research interests include multilevel converters topologies and control, predictive control of power electronics converters, and photovoltaic energy systems.



**RALPH KENNEL** (Senior Member, IEEE) was born in Kaiserslautern, Germany, in 1955. He received the Diploma and Dr.-Ing. (Ph.D.) degrees in electrical engineering from the University of Kaiserslautern, Kaiserslautern, in 1979 and 1984, respectively.

From 1983 to 1999, he worked on several positions with Robert BOSCH GmbH, Germany. Until 1997, he was responsible for the development of servo drives. He was one of the main supporters of

VECON and SERCOS interface, two multi-company development projects for a microcontroller and a digital interface especially dedicated to servo drives. Furthermore, he took actively part in the definition and release of new standards with respect to CE marking for servo drives. From 1997 to 1999, he was responsible for “Advanced and Product Development of Fractional Horsepower Motors” in automotive applications. His main activity was preparing the introduction of brushless drive concepts to the automotive market. From 1994 to 1999, he was a Visiting Professor at the University of Newcastle-upon-Tyne, U.K. From 1999 to 2008, he was a Professor of electrical machines and drives at Wuppertal University, Wuppertal, Germany. Since 2008, he has been a Professor of electrical drive systems and power electronics at the Technical University of Munich, Munich, Germany. His main research interests include sensorless control of ac drives, predictive control of power electronics, and hardware-in-the-loop systems.

Dr. Kennel is a fellow of the Institution of Electrical Engineers (IEE) and a Chartered Engineer in the U.K. Within the IEEE, he is the Treasurer of the Germany Section as well as the ECCE Global Partnership Chair of the Power Electronics Society.



**JOSE RODRIGUEZ** (Life Fellow, IEEE) received the Engineer degree in electrical engineering from the Universidad Técnica Federico Santa María, in Valparaíso, Chile, in 1977, and the Dr.-Ing. degree in electrical engineering from the University of Erlangen, Erlangen, Germany, in 1985.

He has been with the Department of Electronics Engineering, Universidad Técnica Federico Santa María, since 1977, where he was a Full Professor and the President. From 2015 to 2019, he was the

President of the Universidad Andrés Bello in Santiago, Chile. Since 2022, he has been the President of the Universidad San Sebastian in Santiago, Chile. He has coauthored two books, several book chapters, and more than 400 journals and conference papers. His main research interests include multilevel inverters, new converter topologies, control of power converters, and adjustable-speed drives. He is a member of the Chilean Academy of Engineering. He has received a number of best paper awards from journals

of the IEEE. In 2014, he received the National Award of Applied Sciences and Technology from the Government of Chile. In 2015, he received the Eugene Mittelmann Award from the Industrial Electronics Society of the IEEE. From 2014 to 2020, he was included in the list of Highly Cited Researchers published by Web of Science.



**MOHAMED ABDELRAHEM** (Senior Member, IEEE) was born in Assiut, Egypt, in 1985. He received the B.Sc. (Hons.) and M.Sc. degrees in electrical engineering from Assiut University, Assiut, in 2007 and 2011, respectively, and the Ph.D. degree (Hons.) in electrical engineering from the Technical University of Munich (TUM), Munich, Germany, in 2020.

Since 2019, he has been the Head of the Research Group “Renewable Energy Systems” at the Chair of High-Power Converter Systems (HLU), TUM. Since 2020, he has been an Assistant Professor at the Electrical Engineering Department, Assiut University. His research interests include power electronics, predictive and encoderless control of variable-speed wind generators, photovoltaic energy systems, and energy storage systems. In 2020, he received the Walter Gademann Prize from the Faculty of Electrical and Computer Engineering, TUM, in recognition of his excellent Ph.D. dissertation entitled “Predictive Control and Finite-Set Observers for Variable-Speed Wind Generators.” Furthermore, he has received a number of best paper awards from high prestigious international conferences of the IEEE. He is recorded in world’s top 2% scientist’s list by Stanford University.

• • •